HHS Public Access

Author manuscript

J Mol Biol. Author manuscript; available in PMC 2016 March 27.

Published in final edited form as:

J Mol Biol. 2015 March 27; 427(6 0 0): 1211–1223. doi:10.1016/j.jmb.2014.06.016.

Ion Conductance of the Stem of the Anthrax Toxin Channel during Lethal Factor Translocation

Aviva Schiffmiller[1] and **Alan Finkelstein**[1]

[1]Department of Physiology and Biophysics, Albert Einstein College of Medicine, 1300 Morris Park Ave, Bronx, NY 10461, USA

Abstract

The tripartite anthrax toxin consists of protective antigen (PA), lethal factor (LF), and edema factor (EF). PA_{63} (the 63 kDa, C-terminal part of PA) forms heptameric channels in cell membranes that allow for the transport of LF and EF into the cytosol. These channels are mushroom-shaped, with a ring of seven phenylalanine residues (known as the phenylalanine clamp) lining the junction between the cap and stem. It is known that when LF is translocated through the channel, the phenylalanine clamp creates a seal that causes an essentially complete block of conduction. In order to examine ion conductance in the stem of the channel, we used Venus yellow fluorescent protein (YFP) as a molecular stopper to trap LF_N (the 30 kDa, 263-residue N-terminal segment of LF), and various truncated constructs of LF_N, in mutant channels in which the phenylalanine clamp residues were mutated to alanines. Here we present evidence that ion movement occurs within the channel stem (but is stopped, of course, at the phenylalanine clamp) during protein translocation. Furthermore, we also propose that the lower region of the stem plays an important role in securing peptide chains during translocation.

Keywords

protein translocation; ion-conducting channels; phenylalanine clamp; conductance block; single channels

Introduction

Anthrax toxin consists of three proteins: edema factor (EF; 89 kDa), lethal factor (LF; 90 kDa), and protective antigen (PA; 83 kDa). The former two are enzymes (EF is an adenylate cyclase[1] and LF is a protease[2, 3]) which exert their toxic effects when present in the cell' cytosol. They can gain access to the cytosol, however, only in binary combination with PA. PA forms channels in cell membranes that facilitate the transport of EF and LF into cells

Corresponding author: Aviva Schiffmiller, aviva.schiffmiller@phd.einstein.yu.edu, Phone: 718-430-3169, Fax: (718) 430-8819, Albert Einstein College of Medicine, Ullmann 205, 1300 Morris Park Ave, Bronx, NY 10461, USA.

(for a general review of anthrax toxin, see reference 4). Channel formation begins when PA_{83} binds to a receptor on the cell surface and is cleaved by a furin-like protease, which detaches a 20 kDa segment from the N-terminus. The remaining 63 kDa (PA_{63}) segment stays attached to the receptor and heptamerizes[4] (or octamerizes[5]) to form a prepore that can bind a maximum of three ligands (EF/LF). These ligand-receptor complexes are then taken up into the cell via endocytosis and end up in an acidic vesicular compartment. The low pH in this vesicle causes the prepore to form the $(PA_{63})_7$ channel in the vesicular membrane, through which LF and EF can then pass into the cytosol[4]. Understanding the mechanism by which this translocation occurs may elucidate general principles of protein translocation across cell membranes.

The $(PA_{63})_7$ channel (Figure 1A) is mushroom-shaped, with a globular cap domain and a cylindrical stem domain[6, 7]. The stem is an extended 14-stranded β-barrel, roughly 100 Åring; long (25 Åring; crossing the lipid bilayer and 75 Åring; extending from it)[8, 9]. $(PA_{63})_7$ can be reconstituted in a planar lipid bilayer membrane, forming cation-selective channels with a conductance of ~55 pS (in 100 mM KCl, pH 5.5)[10]. It has been shown that LF_N (the 30 kDa, 263-residue N-terminal segment of LF), as well as whole EF and LF, can be translocated through these channels, N-terminus first, by applying positive voltages to the *cis* solution (the solution to which $(PA_{63})_7$ was added)[11, 12] as well as by establishing a pH gradient across the membrane[13]. In this system, LF_N (in the fully extended state[14]) passes from the *cis* solution, through the channel stem, and into the opposite *trans* solution[15].

A ring of seven phenylalanine residues (F427), known as the “phenylalanine clamp” (φ-clamp), lies near the junction between the cap and stem of $(PA_{63})_7$ and is important for LF_N translocation. The bulky φ-clamp residues form a narrow “iris” in the channel that binds LF_N stably in the lumen, causing an effectively complete block in conduction[10]. It is not known, however, whether the *stem* of the channel allows for any conduction during LF_N translocation; that is, whether ions can move from the *trans* entrance of the channel into the stem. This question has important implications regarding the forces involved in voltage-driven translocation: namely, whether the electric field is focused at the φ-clamp (if ions can enter the stem) or decays along the length of the channel (if ions cannot enter the stem). In this paper, we demonstrate that in the absence of the φ-clamp, ion conductance is not completely blocked in the stem of the channel when the stem is occupied by LF_N. That is, the electrical resistance of the stem is much lower than that across the φ-clamp. We also find that the lower region of the stem (near the *trans* end of the channel) appears to better secure the translocating species in the channel than does the upper region.

General Strategy

The φ-clamp completely blocks ion conduction during LF_N translocation. Thus, with the φ-clamp present we cannot determine whether ions can enter the stem from the *trans* solution when it is occupied by LF_N. Mutating the phenylalanine residues of the φ-clamp to alanines removes the block[10] and thereby allowed us to observe to what extent, if any, ions may permeate the stem of the channel during LF_N translocation.

To anchor LF_N in the stem and prevent its complete translocation, we attached YFP (yellow fluorescent protein) to the C-terminus of LF_N (Figure 1B). YFP acted as a molecular stopper because it was too large to enter the stem of the anthrax toxin channel[14] (even when the φ-clamp was mutated). This allowed us to trap the translocating species in the channel at positive voltages, since LF_N-YFP was unable to pass out into the *trans* solution (YFP is assumed to be stopped at the φ-clamp; for a comprehensive explanation of this strategy, see reference 14). In addition to generating LF_N-YFP and His-LF_N-YFP (His_6-tagged LF_N-YFP), we also performed deletions from the C-terminus of LF_N (as described in reference 14) in order to create a series of truncated versions of both LF_N-YFP and His-LF_N-YFP (Figure 2), which are too short to traverse the entire length of the channel (as measured from the φ-clamp to the bottom of the stem).

We performed macroscopic and single-channel electrophysiological experiments using mutant $(PA_{63})_7$ channels in which the phenylalanine residues of the φ-clamp were mutated to less bulky alanine residues ($(PA_{63}F427A)_7$). These mutant channels have a conductance of ~110 pS (in 100 mM KCl, pH 5.5)[10]. We used *cis* positive voltages of +20 mV and +50 mV to drive both the full-length and truncated constructs into $(PA_{63}F427A)_7$ channels (Figures 1B and 1C) in planar lipid bilayers in order to observe the extent of ion conduction in the channel stem when either fully or partially occupied by an inserted protein segment. At +50 mV, LF_N and the His_6-tag are expected to be fully extended into the channel; the degree of extension at +20 mV is not clear[14].

Results

Cis effect of LF_N-YFP, His-LF_N-YFP, and truncated constructs on conductance of $(PA_{63}F427A)_7$ channels

Macroscopic experiments—*Cis* addition of saturating amounts of LF_N-YFP to membranes containing hundreds of $(PA_{63}F427A)_7$ channels (see Figure 3 for a typical record) yielded a ~50-fold reduction in conductance at +50 mV, which was noticeably less than the ~300-fold reduction in conductance observed after *cis* addition of LF_N-YFP to membranes containing WT $(PA_{63})_7$ channels (Figure 4). This difference was even more pronounced at +20 mV (a voltage at which LF_N is not expected to be completely unfolded and/or completely extended through the channel[14,15]), where there was only a ~6-fold reduction in conductance in the mutant channel and a ~90-fold reduction in the WT channel (Figure 4). *Cis* addition of His-LF_N-YFP to both WT and mutant channels yielded comparable results, with much greater block of WT than of mutant channels (Figure 4).

We next determined the macroscopic block in conductance produced by truncated versions of LF_N-YFP and His-LF_N-YFP. The distance required to span the length of the channel, from the φ-clamp to the bottom of the stem, is approximately 120 Åring; (YFP is presumed to be stopped at the φ-clamp when these constructs are driven into the channels at positive voltages[14]). The His-tagged series of truncated constructs (Figure 5) that did not span the entire length of the stem ranged from lengths of 72 Åring; (His-YFP, which is just YFP with a His_6-tag attached) to 119 Åring; (His-LF_N (1–10)-YFP, which is YFP with three linker residues, the first 10 residues of LF_N, and a His_6-tag). These lengths are based on each residue spanning a distance of ~3.6 Åring; in an extended peptide chain[14, 16]. We also

created a construct that was 202 Åring; long (His-LF_N (1–33)-YFP), which is long enough to extend past the bottom of the channel when fully extended, but still much shorter than full-length His-LF_N-YFP (1030 Åring;).

The *cis* effect of the His_6-tagged series of truncated constructs on $(PA_{63}F427A)_7$ channels is shown in Figure 5. Overall, as the length of the construct increased, there was a greater block in conductance at both +20 mV and +50 mV. Additionally, the block in conductance produced by these constructs was less than that observed with full-length His-LF_N-YFP (Figure 4) at both +20 mV and + 50 mV.

The *cis* effect of truncated LF_N-YFP constructs on the conductance of $(PA_{63}F427A)_7$ channels at +20 mV and +50 mV (Figure 6) was similar to the overall effect observed with truncated His-LF_N-YFP constructs (Figure 5). While the general trend of the extent of the block increasing with the length of the construct holds true here as well, the His-tagged series produced a greater reduction in conductance (Figure 5). Compare, for example, the 5-fold block in conductance produced by the *cis* addition of LF_N(1–23)-YFP (108Åring; in length) to $(PA_{63}F427A)_7$ channels at +50 mV (Figure 6) versus the 10-fold block produced by His-LF_N(1–23)-YFP (also 108Åring; in length; Figure 5). As the anthrax toxin channel is cation-selective, the greater block in conductance produced by the His-tagged series may be due to the repulsion of cations by the six consecutive histidine residues of the His_6-tag, assuming that the cation selectivity of the peptide-occupied stem is comparable to that of the unoccupied stem.

Single-channel experiments—The *cis* addition of full-length LF_N-YFP (or His-LF_N-YFP) to $(PA_{63}F427A)_7$ channels produced, at the macroscopic level, less of a block in conductance than when added to WT $(PA_{63})_7$ channels (Figure 4). This can be interpreted in one of two ways. It is possible that this difference reflects the relative times that these channels remain occupied by LF_N. However, it is also possible that this difference reflects a discrepancy in the degree of block when a channel is occupied by LF_N. To distinguish between these two possibilities, we performed single-channel experiments.

Single-channel experiments (Figure 7) revealed that LF_N-YFP remains mostly secure in the $(PA_{63}F427A)_7$ channel (as in the wild-type channel) at both +20 mV and +50 mV; thus, the residual ion conductance observed at the macroscopic level must be due to the presence of small intermediate conductance states that are not observed in the WT channel, but which we see in the mutant channel (Figure 7). Therefore, these results indicate that there is indeed a “leak” in the stem of the anthrax toxin channel that allows ions to enter it (from the *trans* side) during LF_N translocation. Note that while this small residual conductance may be difficult to discern at the single-channel level, particularly at +50 mV, it is easily measured at the macroscopic level (Figure 4). Similar single-channel records were obtained for His-LF_N-YFP in both mutant and WT channels (not shown).

On the other hand, single-channel experiments demonstrated that the incomplete block in conductance observed with the truncated His-LF_N-YFP and LF_N-YFP constructs is a reflection of both the relative amount of time the peptide chain occupies the channel as well as small intermediate states of conductance even when the chain is secure in the channel

(Figures 8 and Figure 9). Experiments with the shortest truncated His-LF_N-YFP constructs revealed that there is quite a bit of flickering in and out of the channel at both +20 mV and +50 mV (Figure 8), which presumably indicates that the peptide chain is not secure in the channel. However, as the length of the His_6-tagged construct increases, the chain appears to be far more secure in the channel, particularly at +50 mV. For example, His-LF_N (1–7)-YFP, which produced only a 10-fold reduction in macroscopic conductance at +50 mV, hardly flickers out of the channel at all at this voltage (Figure 8). (Importantly, the same mean fractional block of conductance was observed on the single-channel level as on the macroscopic level, ~90%.) However, note that at least some of the residual conductance observed with His-LF_N (1–7)-YFP may be attributed to an incomplete block in conductance even when the peptide chain is secure within the channel. Indeed, there appear to be two blocked substates at +50 mV: one where ~ 90% of the open-channel conductance is blocked and one where closer to 100% of the open-channel conductance is blocked. The first substate appears the majority of the time. A similar incompletely-blocked substate is observed in experiments with the truncated LF_N-YFP constructs as well (Figure 9).

Trans effect of His-YFP and LF_N (1–16)-YFP constructs on conductance of $(PA_{63}F427A)_7$ channels

There were two motivating factors for studying the *trans* effect of selected truncated His-LF_N-YFP and LF_N-YFP constructs on the conductance of $(PA_{63}F427A)_7$ channels. The first was to ensure that the β-barrel structure of the $(PA_{63}F427A)_7$ channel stem was not significantly perturbed by the φ-clamp mutation. If the *trans* addition of truncated constructs that were not long enough to reach the φ-clamp (from the bottom of the stem) produced similar blocking effects in both mutant and WT channels, it would indicate that the stem of the $(PA_{63}F427A)_7$ channel was structurally intact.

The second factor was that the single-channel *cis* experiments with truncated His-LF_N-YFP (Figure 8) seemed to indicate that the lower region of the channel stem is important for securing the translocating species in the channel. Note that His-YFP, which is 72 Åring; long (and spans almost 2/3 of the ~120 Åring; distance from the φ-clamp to the bottom of the stem), flickers in and out of the channel rapidly. As the length of the construct extends further into the lower region of the channel stem, the construct hardly pops out of the channel at all. We therefore anticipated that His-YFP and LF_N (1–16)-YFP (82.8 Åring; long) would be held more securely in the channel when added to the *trans* side instead of the *cis* side.

Macroscopic experiments—In *trans* experiments, the voltage protocol is reversed, so that negative voltages produce blocking and positive voltages produce unblocking. We were unable to observe the blocking effect produced at −50 mV due to the intrinsic voltage-dependent gating of these channels. However, even at −20 mV we observed a stark difference between the block produced by His-YFP and LF_N (1–16)-YFP when driven into $(PA_{63}F427A)_7$ channels from the *trans* side versus the *cis* side.

At the macroscopic level, His-YFP produced a ~6-fold reduction in conductance when added to the *trans* side of $(PA_{63}F427A)_7$ channels at −20 mV (Figure 10A), as opposed to

the *cis* effect of a ~2-fold reduction at +20 mV (Figure 5). Likewise, whereas we observed only a ~2.5-fold block in conductance when adding LF_N(1–16)-YFP to the *cis* side of $(PA_{63}F427A)_7$ channels at +20 mV (Figure 6), *trans* addition produced an ~11-fold block in conductance at −20 mV (Figure 11A). We repeated these experiments with WT channels and obtained comparable results (data not shown).

Single-channel experiments—At the single-channel level, the *trans* addition of His-YFP to $(PA_{63}F427A)_7$ channels revealed that the channel stem is able to secure His-YFP most of the time (Figure 10B). It is clear that the peptide chain occupies the channel for a far greater amount of time when added from the *trans* side instead of from the *cis* side (compare Figure 10B to Figure 8), supporting our proposal that the lower region of the stem is important for securing the translocating species in the channel. Single-channel *trans* experiments also confirmed that LF_N(1–16)-YFP is able to remain securely in the mutant channel for the majority of the time (Figure 11B).

We once again repeated these experiments using WT channels and obtained records that were quite similar to the experiments with the mutant channels for both His-YFP (Figure 10B) and LF_N (1–16)-YFP (Figure 11B). Importantly, LF_N (1–16)-YFP produced intermediate states of conductance in both WT and mutant channels, which seems to indicate that the β-barrel structure of the $(PA_{63}F427A)_7$ channels has not been grossly perturbed.

Discussion

In this paper, we have addressed the question of whether the stem of the mushroom-shaped anthrax toxin channel allows for ion movement within it during protein translocation. We found that whereas there is complete ion conduction block at the φ-clamp, there is substantial, but incomplete, block by the polypeptide chain in the stem, and we further characterized the extent of the macroscopic block as a function of the length of the peptide chain. The block may be both a steric one and an electrostatic one arising from charges on the polypeptide chain. This latter, in fact, may account for the larger blocking effects produced by the constructs having a His_6-tag at the N terminus (compare Figures 5 and 6). We also observe a greater block at +50 mV than at +20 mV, since although the peptide chain likely adopts a fully-extended configuration inside the channel at both voltages, at +20 mV the chain is expected to spend less time further down in the channel than at +50 mV, due to Brownian motion. All of the implications of this finding for LF_N translocation through the $(PA_{63})_7$ channels are not yet clear, but one thing is certain: in considering voltage-driven translocation, one must now recognize that most of the applied voltage is dropped across the φ-clamp and not along the stem.

It is possible that the mutation of the phenylalanines at the φ-clamp to alanines has modified the channel' stem so that the incomplete conductance block there does not hold true for the wild-type stem. This, however, is unlikely, as in both macroscopic and single-channel (Figures 10B and 11B) experiments, the *trans* addition of His-YFP and LF_N(1–16)-YFP produced comparable results on WT $(PA_{63})_7$ and $(PA_{63}F427A)_7$ channels.

That there exists an incomplete block of conductance in the channel stem during protein translocation has been suggested previously in studies of pH-driven translocation in WT $(PA_{63})_7$ and $(PA_{63}F427A)_7$ channels[13]. The rate of pH-driven translocation is significantly slowed when the φ-clamp is mutated to alanines; it has been proposed that this effect is a result of the collapse of the pH-gradient due to a small amount of protons "leaking" through the mutant channel[13, 17]. Our demonstration that there is indeed a small residual conductance in the channel stem certainly bolsters this claim. Furthermore, prior voltage-driven translocation studies have also demonstrated evidence of leaky sub-conductance states; the *cis* addition of LF_N to $(PA_{63}F427A)_7$ at +20 mV yields intermediate states of conductance[10].

In addition to the incomplete block of ion conductance in the channel stem during LF_N translocation, another feature of the stem is revealed from our experiments with truncated versions of His-LF_N-YFP that were not long enough to completely transverse the stem. Namely, the securing of the polypeptide chain within the channel stem appears to reside in the lower third of the stem. This was evidenced from the experiments in which His-LF_N-YFP constructs of various lengths were added to the *cis* solution (Figure 8) and was confirmed by the addition of the short His-YFP to the *trans* solution (Figure 10B). The implication is that the lumen of the stem narrows in its lower region, although one cannot preclude specific binding interactions between residues in the stem and those on the polypeptide chain. We must also acknowledge the possibility of YFP partially unfolding, which would obscure the length of the chain that is present in the channel, but we believe this is unlikely (for a further discussion of this matter, see reference 14).

We cannot ignore the possibility that the large block in conductance produced when adding His-YFP (or LF_N(1–16)-YFP) to the *trans* side of both mutant and WT channels is due simply to the binding of YFP to residues on the *trans* end of the channel, or to the lipid bilayer adjacent to the *trans* entrance to the channel. However, we believe these scenarios to be unlikely. First, in experiments in which the bottom-most residues (F313 and F314) of the $(PA_{63})_7$ channel stem were mutated to alanines, adding His-YFP to the *trans* side of these channels produced the same degree of block observed with WT channels (unpublished results). Second, studies have shown that YFP does not have strong associations with the lipid bilayers of plasma membranes[18].

One last point: the single-channel records reported here are highly filtered (10–15 Hz) and therefore are not very revealing of the magnitudes of the sub-states and their dwell times. Future experiments at much higher time resolution are contemplated. These will give a finer picture of the Brownian motion and drift of the polypeptide chain within the stem.

Materials and Methods

Molecular biology and protein purification

His-LF_N-YFP protein, with a His_6-tag attached to the N-terminus of LF_N and Venus YFP fused at its C terminus, was constructed as described previously[14]. Briefly, the pET-15b plasmid (Novagen) encodes a thrombin-cleavable His_6-tag sequence (Merck) into which

was cloned LF_N residues 1–263, followed by a serine-glycine-serine linker, followed by Venus YFP, for a total insert of 503 residues.

In order to create truncated constructs, complementary mutagenic oligonucleotides were used to delete central segments of His-LF_N-YFP. Using the QuikChange Site-Directed Mutagenesis kit, the following constructs were generated (in all of these constructs, the 20-residue His_6-tag is attached at the N-terminus and the YFP is attached at the C-terminus): His-YFP (LF_N and the linker residues were deleted), His-YFP (with the linker residues included), His-LF_N(1–3)-YFP, His-LF_N(1–5)-YFP, His-LF_N(1–7)-YFP, His-LF_N(1–10)-YFP, His-LF_N(1–16)-YFP, His-LF_N(1–23)-YFP and His-LF_N(1–33)-YFP (see Figure 2 for representative schematic constructs).

His-LF_N-YFP and the truncated constructs were expressed recombinantly and purified as previously described[10, 12, 14, 19, 20]. Wild-type $(PA_{63})_7$ (trypsin-nicked PA_{83} from which PA_{20} was removed[21]) was a gift from Dr. Sen Zheng. Mutant $(PA_{63}F427A)_7$ was the same sample previously reported[10]. In some of the experiments, the His_6-tags on His-LF_N-YFP and the various truncated constructs were cleaved with thrombin according to the Novagen manual protocol (Figure 2).

Planar lipid bilayers

Planar lipid bilayers were formed via the brush technique[22] across a 0.5 mm hole in a 125-μm-thick Teflon partition. The membranes separated two Lucite compartments that each contained 3 mL of 100 mM KCl, 25 mM potassium-succinate, 1 mM EDTA, pH 5.5. In experiments in which we wished to reduce the noise level further, membranes were formed across a 100-μm diameter aperture in a polystyrene cup[23]; the front compartment contained 1.5 mL of solution and the rear compartment contained 0.75 mL. The individual compartments were stirred using small magnetic stir bars. Agar salt bridges (3M KCl, 3% agar) connected Ag/AgCl electrodes in saturated KCl solutions to the *cis* and *trans* compartments. The membrane-forming solution was 3% diphytanoyl-phosphatidylcholine (Avanti Polar Lipids, Inc.) in *n*-decane; membrane formation was observed visually. All experiments were performed under voltage clamp conditions; voltages are those of the *cis* solution (to which $(PA_{63})_7$ or $(PA_{63}F427A)_7$ prepore heptamer was added) in reference to the *trans* solution (held at virtual ground). Current responses were filtered at 10–15 Hz by a low-pass eight-pole Bessel filter (Warner Instruments) and recorded on a DMP-4B Physiograph chart recorder, as well as an NI USB-6211 Data Acquisition Board (National Instruments) for digital storage[14, 24].

$(PA_{63})_7$ channel formation and conductance block

Following membrane formation, either wild-type $(PA_{63})_7$ or $(PA_{63}F427A)_7$ prepore heptamer was added to the *cis* compartment, which was held at a voltage of +20 mV with respect to the *trans* compartment. When the conductance produced by $(PA_{63})_7$ channel formation reached a steady-state, LF_N-YFP (or His-LF_N-YFP or one of the truncated constructs) was added to the *cis* compartment at near-saturating concentrations (~0.2 μ*M* for His-LF_N-YFP and LF_N-YFP; ~0.47 μ*M* for truncated His-LF_N-YFP and LF_N-YFP constructs). The blocking of the channels by LF_N-YFP or one of its variants was monitored

by the fall in conductance at +20 mV and +50 mV (a typical record is shown in Figure 3). In the *trans* experiments, the voltage was held at −20 mV, and the truncated constructs were added to the *trans* compartment.

The protocol for single-channel experiments was the same, except that only one or two channels were allowed to form (by adding dilute amounts of $(PA_{63})_7$ or $(PA_{63}F427A)_7$ prepore heptamer).

Acknowledgements

We thank Karen Jakes, Paul Kienker, Russell Thomson, and Eshwar Udho for their assistance in performing the experiments described in this paper. We also thank Myles Akabas, Karen Jakes, and Paul Kienker for their helpful comments on the manuscript, and Daniel Basilio for the use of his plasmids.

This work was supported by National Institutes of Health research grant GM 29210.

Abbreviations used in this paper

PA	protective antigen
LF	lethal factor
EF	edema factor
PA_{63}	63 kDa C-terminal portion of PA
$(PA_{63})_7$	the heptameric form of PA_{63}
LF_N	the 30 kDa, 263-residue N-terminal segment of LF
φ-clamp	phenylalanine clamp
YFP	yellow fluorescent protein
LF_N-YFP	LF_N with YFP attached to its C-terminus
His-LF_N-YFP	His_6-tagged LF_N-YFP
$(PA_{63}F427A)_7$	the heptameric form of PA_{63} with an F427A mutation
WT	wild-type

References

1. Leppla SH. Anthrax toxin edema factor: a bacterial adenylate cyclase that increases cyclic AMP concentrations of eukaryotic cells. Proc. Natl. Acad. Sci. U. S. A. 1982; 79:3162–3166. [PubMed: 6285339]
2. Duesbery NS, Webb CP, Leppla SH, Gordon VM, Klimpel KR, Copeland TD, Ahn NG, Oskarsson MK, Fukasawa K, Paull KD, Vande Woude GF. Proteolytic inactivation of MAP-kinase-kinase by anthrax lethal factor. Science. 1998; 280:734–737. [PubMed: 9563949]
3. Vitale G, Pellizzari R, Recchi C, Napolitani G, Mock M, Montecucco C. Anthrax lethal factor cleaves the N-terminus of MAPKKs and induces tyrosine/threonine phosphorylation of MAPKs in cultured macrophages. Biochem. Biophys. Res. Commun. 1998; 248:706–711. [PubMed: 9703991]
4. Young JA, Collier RJ. Anthrax toxin: receptor binding, internalization, pore formation, and translocation. Annu. Rev. Biochem. 2007; 76:243–265. [PubMed: 17335404]

5. Kintzer AF, Thoren KL, Sterling HJ, Dong KC, Feld GK, Tang II, Zhang TT, Williams ER, Berger JM, Krantz BA. The protective antigen component of anthrax toxin forms functional octameric complexes. J. Mol. Biol. 2009; 392:614–629. [PubMed: 19627991]
6. Nguyen TL. Three-dimensional model of the pore form of anthrax protective antigen. Structure and biological implications. J. Biomol. Struct. Dyn. 2004; 22:253–265. [PubMed: 15473701]
7. Katayama H, Janowiak BE, Brzozowski M, Juryck J, Falke S, Gogol EP, Collier RJ, Fisher MT. GroEL as a molecular scaffold for structural analysis of the anthrax toxin pore. Nat. Struct. Mol. Biol. 2008; 15:754–760. [PubMed: 18568038]
8. Nassi S, Collier RJ, Finkelstein A. PA_{63} channel of anthrax toxin: an extended beta-barrel. Biochemistry. 2002; 41:1445–1450. [PubMed: 11814336]
9. Benson EEL, Huynh PD, Finkelstein A, Collier RJ. Identification of residues lining the anthrax protective antigen channel. Biochemistry (Easton). 1998; 37:3941–3948.
10. Krantz BA, Melnyk RA, Zhang S, Juris SJ, Lacy DB, Wu Z, Finkelstein A, Collier RJ. A phenylalanine clamp catalyzes protein translocation through the anthrax toxin pore. Science. 2005; 309:777–781. [PubMed: 16051798]
11. Zhang S, Finkelstein A, Collier RJ. Evidence that translocation of anthrax toxin' lethal factor is initiated by entry of its N terminus into the protective antigen channel. Proc. Natl. Acad. Sci. U. S. A. 2004; 101:16756–16761. [PubMed: 15548616]
12. Zhang S, Udho E, Wu Z, Collier RJ, Finkelstein A. Protein translocation through anthrax toxin channels formed in planar lipid bilayers. Biophys. J. 2004; 87:3842–3849. [PubMed: 15377524]
13. Krantz BA, Finkelstein A, Collier RJ. Protein translocation through the anthrax toxin transmembrane pore is driven by a proton gradient. J. Mol. Biol. 2006; 355:968–979. [PubMed: 16343527]
14. Basilio D, Jennings-Antipov LD, Jakes KS, Finkelstein A. Trapping a translocating protein within the anthrax toxin channel: implications for the secondary structure of permeating proteins. J. Gen. Physiol. 2011; 137:343–356. [PubMed: 21402886]
15. Finkelstein A. Proton-coupled protein transport through the anthrax toxin channel. Philos. Trans. R. Soc. Lond. B. Biol. Sci. 2009; 364:209–215. [PubMed: 18957378]
16. Dickerson, RE.; Geis, I. The structure and action of proteins. Menlo Park, CA: Benjamin/ Cummings Publishing Company; 1969.
17. Basilio D, Juris SJ, Collier RJ, Finkelstein A. Evidence for a proton–protein symport mechanism in the anthrax toxin channel. J. Gen. Physiol. 2009; 133:307–314. [PubMed: 19204186]
18. Vazquez F, Matsuoka S, Sellers WR, Yanagida T, Ueda M, Devreotes PN. Tumor suppressor PTEN acts through dynamic interaction with the plasma membrane. Proc. Natl. Acad. Sci. U. S. A. 2006; 103:3633–3638. [PubMed: 16537447]
19. Pimental RA, Christensen KA, Krantz BA, Collier RJ. Anthrax toxin complexes: heptameric protective antigen can bind lethal factor and edema factor simultaneously. Biochem. Biophys. Res. Commun. 2004; 322:258–262. [PubMed: 15313199]
20. Krantz BA, Trivedi AD, Cunningham K, Christensen KA, Collier RJ. Acid-induced unfolding of the amino-terminal domains of the lethal and edema factors of anthrax toxin. J. Mol. Biol. 2004; 344:739–756. [PubMed: 15533442]
21. Blaustein RO, Koehler TM, Collier RJ, Finkelstein A. Anthrax toxin: channel-forming activity of protective antigen in planar phospholipid bilayers. Proc. Natl. Acad. Sci. U. S. A. 1989; 86:2209–2213. [PubMed: 2467303]
22. Mueller P, Rudin DO, Tien HT, Wescott WC. Methods for the formation of single bimolecular lipid membranes in aqueous solution. J. Phys. Chem. 1963; 67:534–535.
23. Wonderlin W, Finkel A, French R. Optimizing planar lipid bilayer single-channel recordings for high resolution with rapid voltage steps. Biophys. J. 1990; 58:289–297. [PubMed: 1698470]
24. Udho E, Jakes KS, Buchanan SK, James KJ, Jiang X, Klebba PE, Finkelstein A. Reconstitution of bacterial outer membrane TonB-dependent transporters in planar lipid bilayer membranes. Proc. Natl. Acad. Sci. U. S. A. 2009; 106:21990–21995. [PubMed: 19959664]
25. Senzel L, Huynh PD, Jakes KS, Collier RJ, Finkelstein A. The diphtheria toxin channel-forming T domain translocates its own NH2-terminal region across planar bilayers. J. Gen. Physiol. 1998; 112:317–324. [PubMed: 9725891]

26. Howorka S, Bayley H. Probing distance and electrical potential within a protein pore with tethered DNA. Biophys. J. 2002; 83:3202–3210. [PubMed: 12496089]

Highlights

- Ion conduction in the stem of the anthrax toxin channel is analyzed.
- Block in conductance in the channel stem is incomplete during protein translocation.
- The lower region of the stem may secure the peptide chain during translocation.

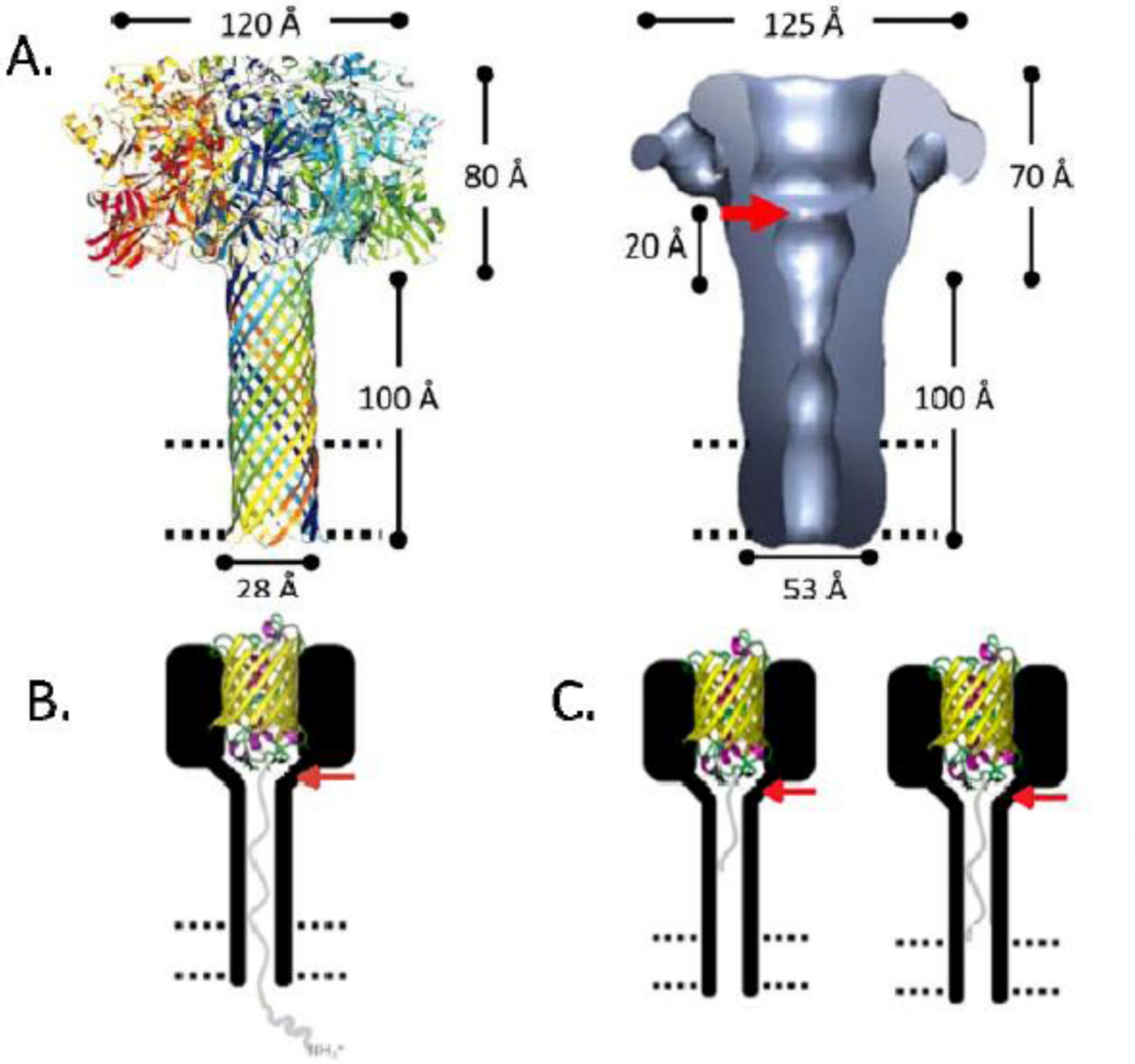

Figure 1.

A[14]*Left:* Model of $(PA_{63})_7$[6]*Right:* Structure of $(PA_{63})_7$, determined by negative-stain electron microscopy (~25 Åring; resolution)[7]. The red arrow denotes the presumed position of the φ-clamp; the 20 Åring; bar represents the distance from the φ-clamp to the presumed beginning of the stem; the dashed parallel lines represent the lipid bilayer. **B**. LF_N-YFP trapped in $(PA_{63}F427A)_7$ at +50 mV. YFP is represented as a yellow β-barrel; LF_N is represented as a grey line; the bilayer is represented as parallel dashed lines. The red arrow indicates the position at which the phenylalanine residues of the φ-clamp were mutated to alanine residues (adapted from reference 14). **C**. Truncated versions of LF_N-YFP trapped in $(PA_{63}F427A)_7$ at +50 mV. YFP is represented as a yellow β-barrel; LF_N is represented as a

grey line; the bilayer is represented as parallel dashed lines. The red arrow indicates the position at which the phenylalanine residues of the φ-clamp were mutated to alanine residues (adapted from reference 14).

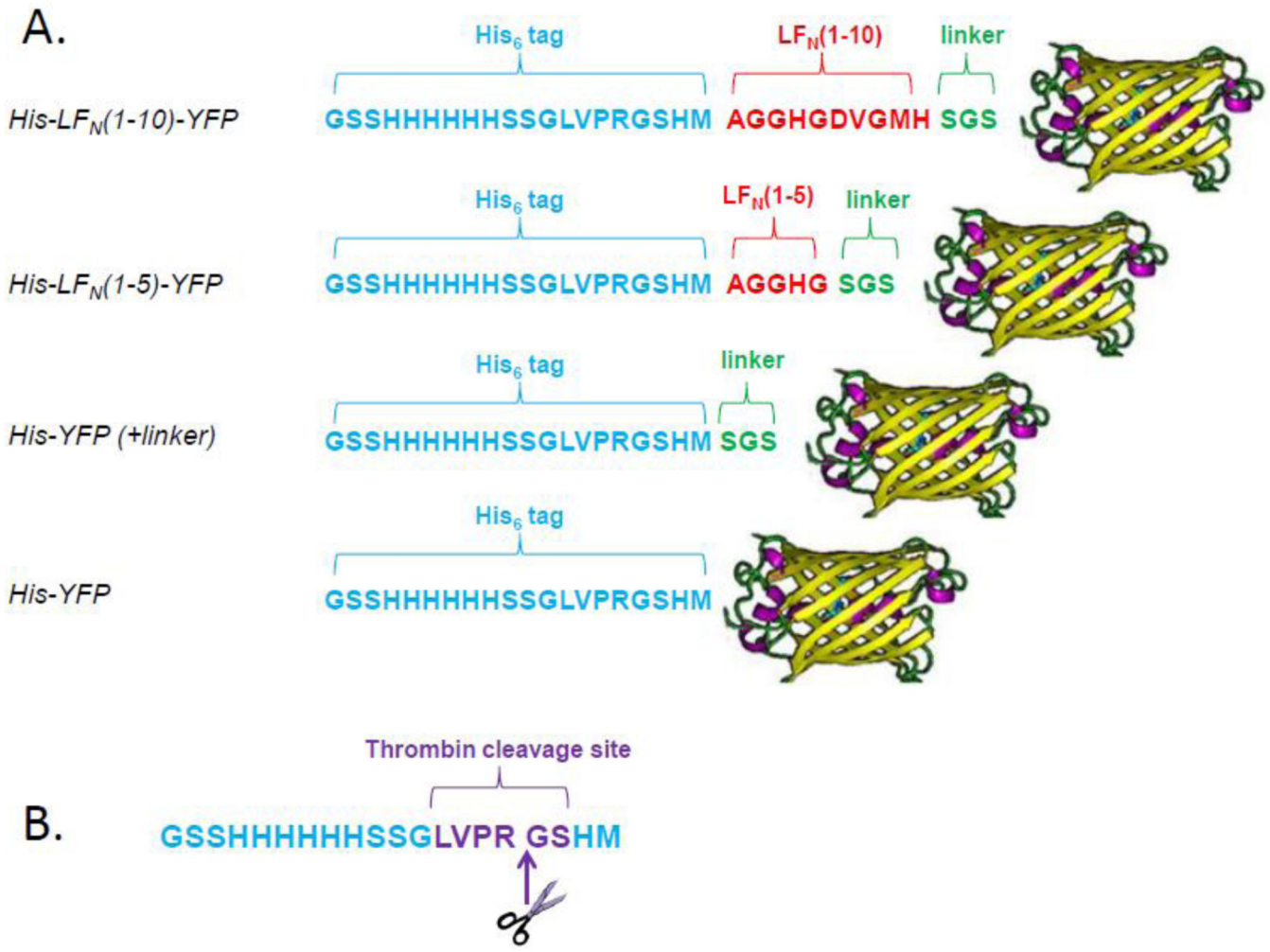

Figure 2.

A. Schematic of selected truncated His-LF_N-YFP constructs. The N-terminal 20-residue His_6-tag is shown in blue, LF_N residues are shown in red, linker residues are shown in green, and the C-terminal YFP is shown as a yellow β-barrel. **B**. 20-residue His_6-tag. Note that the N-terminal methionine residue encoded by pET-15b is not present, as it is removed during protein expression[25]. The site of thrombin cleavage is shown in purple, with the cleavage taking place between the arginine and glycine residues. Thrombin treatment removes the first 16 residues of the tag, leaving behind four residues (Gly-Ser-His-Met).

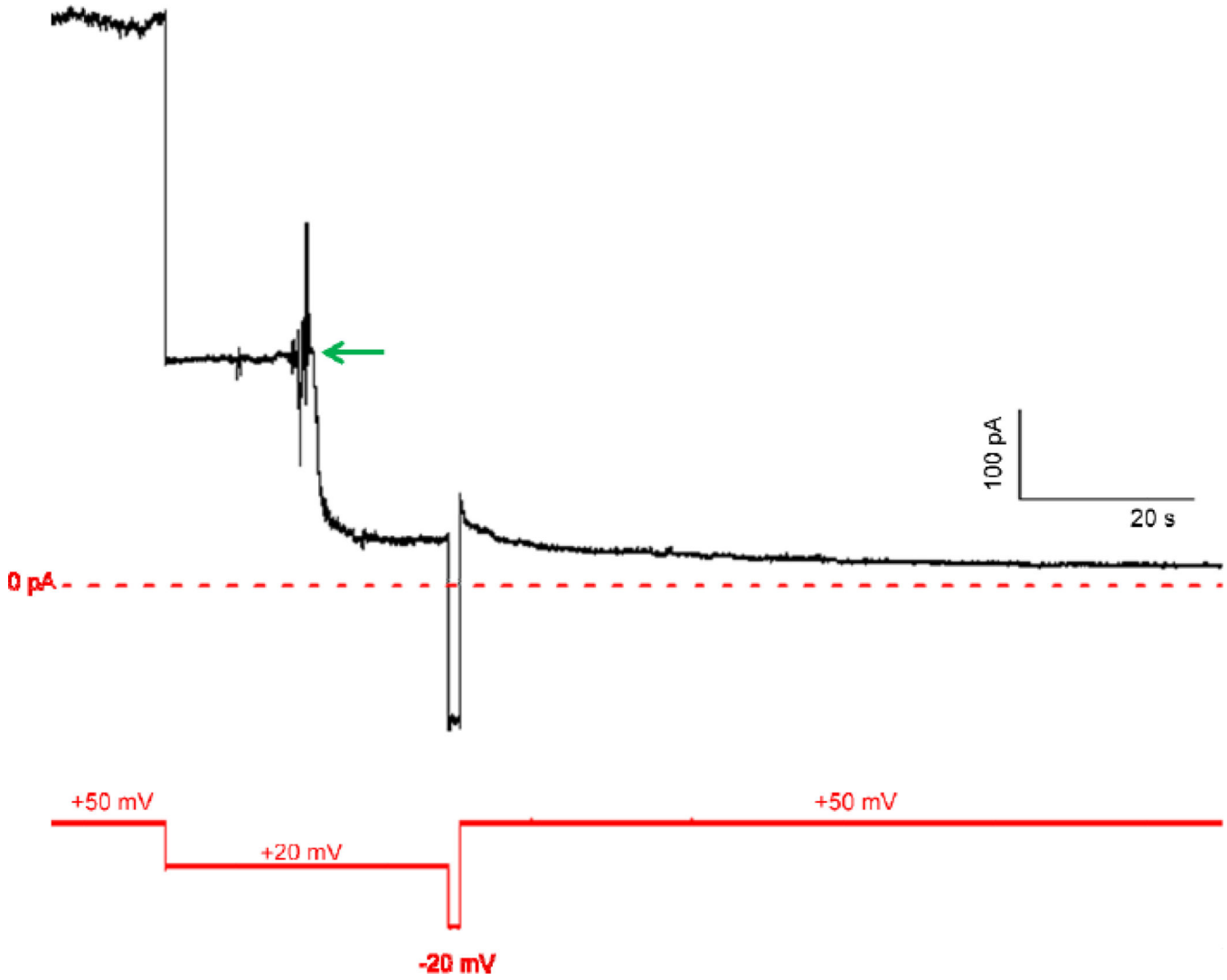

Figure 3.

Record of *cis* addition of LF_N-YFP to a membrane containing $(PA_{63}F427A)_7$ channels. After the current (shown as a black line) produced by $(PA_{63}F427A)_7$ channels reached a steady-state at both +50 mV and +20 mV, LF_N-YFP was added at the green arrow to a final concentration of ~0.2 μM (voltage held at +20 mV), reducing the current by a factor of ~6. After the current reached a new steady-state, the channels were unblocked by applying a voltage of −20 mV, and subsequently re-blocked by applying a voltage of +50 mV, causing the current to be reduced by a total factor of ~50. Voltage is shown as a solid red line; the zero baseline of current is shown as a dashed red line.

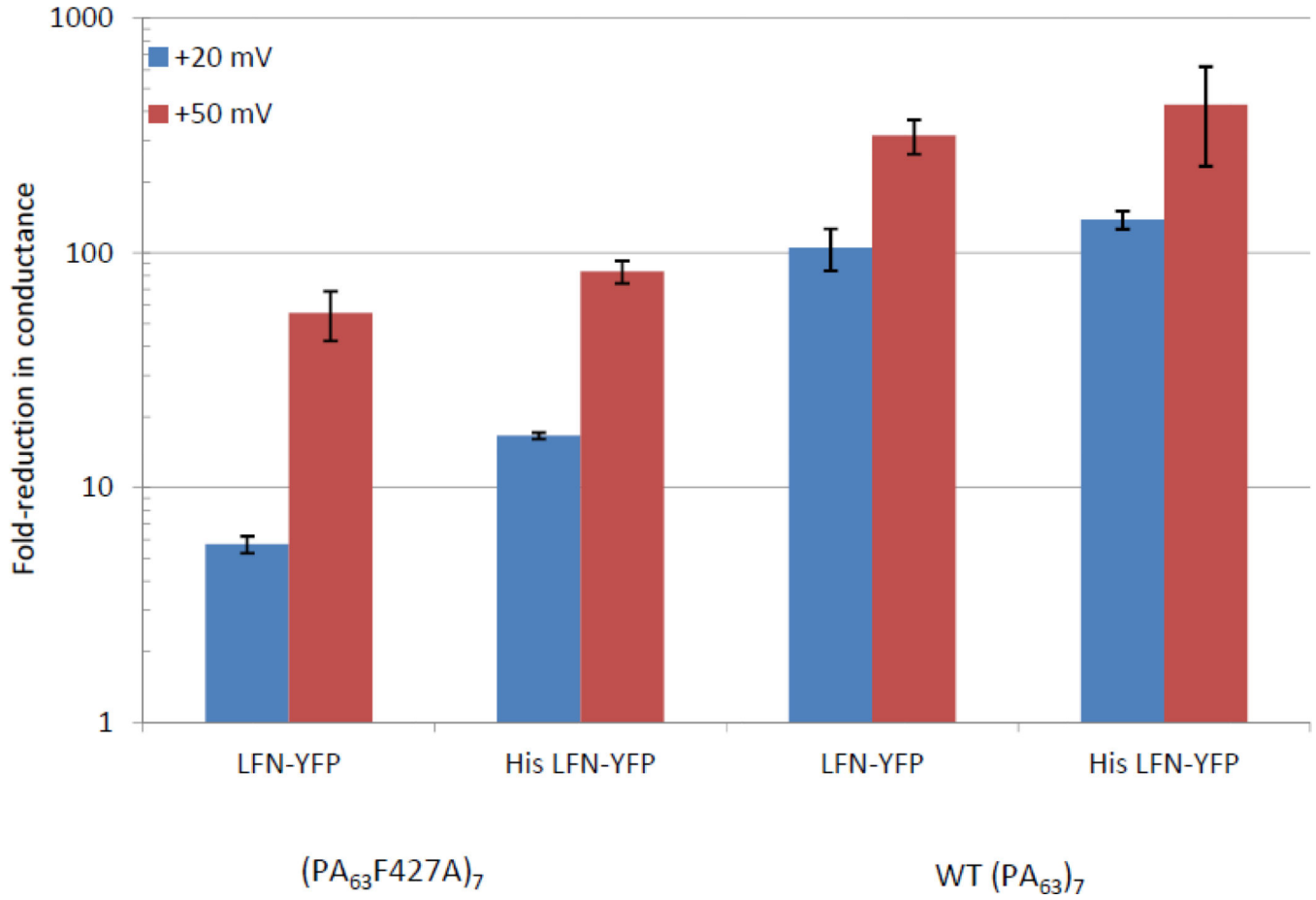

Figure 4.

Cis effect of saturating concentrations (~0.2 μM) of LF_N-YFP and His-LF_N-YFP on conductance of $(PA_{63}F427A)_7$ and WT $(PA_{63})_7$ channels at +20 mV and +50 mV. All experiments were performed in triplicate; error bars represent standard error.

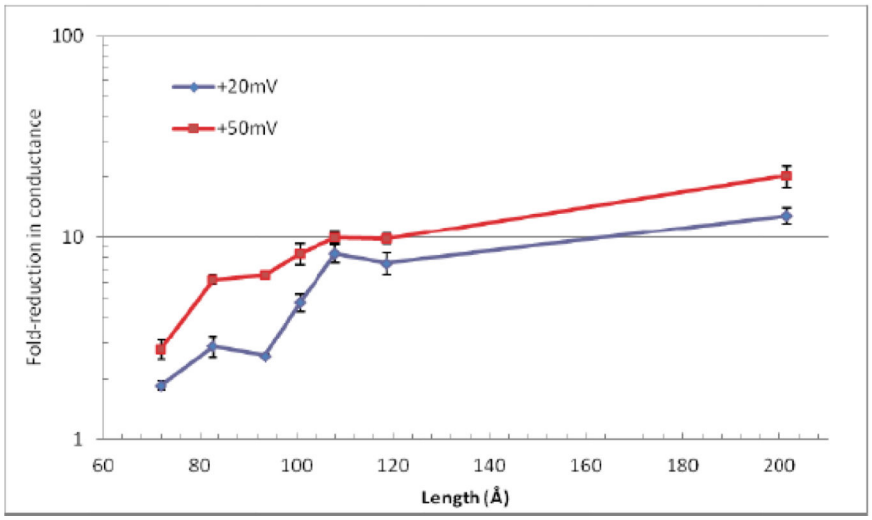

Construct	# aa	Length (Å)
His-YFP	20	72
His-YFP(+SGS linker)	23	82.8
His-LF_N(1-3)-YFP	26	93.6
His-LF_N(1-5)-YFP	28	100.8
His-LF_N(1-7)-YFP	30	108
His-LF_N(1-10)-YFP	33	118.8
His-LF_N(1-33)-YFP	56	201.6

Figure 5.

Left. Cis effect of saturating concentrations (~0.47 μM) of truncated His-LF_N-YFP constructs on conductance of $(PA_{63}F427A)_7$ channels at +20 and +50 mV. All experiments were performed in triplicate; error bars represent standard error (bars that are not visible are small enough that they are obscured by the marker). *Right*. List of truncated His-LF_N-YFP constructs and the number of amino acids/length of each (not including YFP, which is presumed not to unwind when positive voltages are applied). All of the constructs contain a 20-residue His_6-tag, as well as a Ser-Gly-Ser linker before YFP, except for His-YFP (the first construct on the list), which is just the His_6-tag attached directly to YFP.

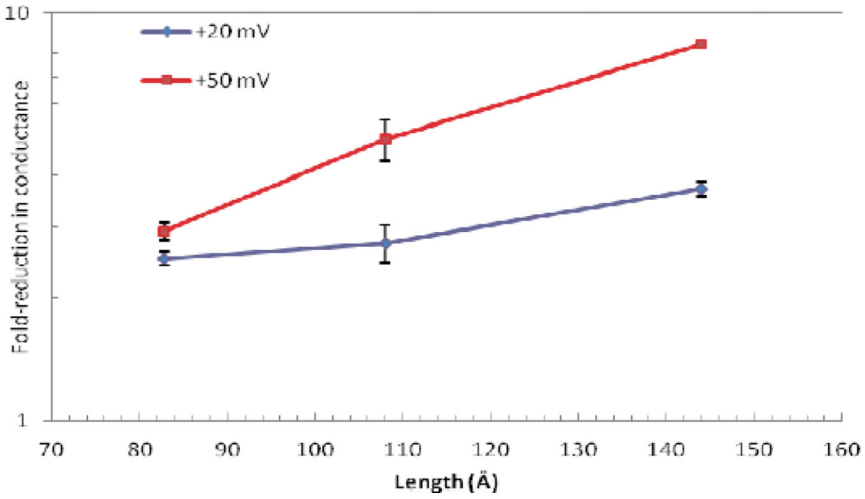

Construct	# aa	Length (Å)
LF_N(1-16)-YFP	23	82.8
LF_N(1-23)-YFP	30	108
LF_N(1-33)-YFP	40	144

Figure 6.

Left. Cis effect of saturating concentrations (~0.47 ~M) of truncated LF_N-YFP constructs on the conductance of $(PA_{63}F427A)_7$ channels at +20 mV and +50 mV. All experiments were performed in triplicate; error bars represent standard error (bars that are not visible are small enough that they are obscured by the marker). *Right*. List of truncated LF_N-YFP constructs and the number of amino acids/length of each (not including YFP, which is presumed not to unwind when positive voltages are applied). All of the constructs contain four residual residues from the His_6-tag (which was cleaved by thrombin), followed by the specified LF_N residues as well as a Ser-Gly-Ser linker before YFP.

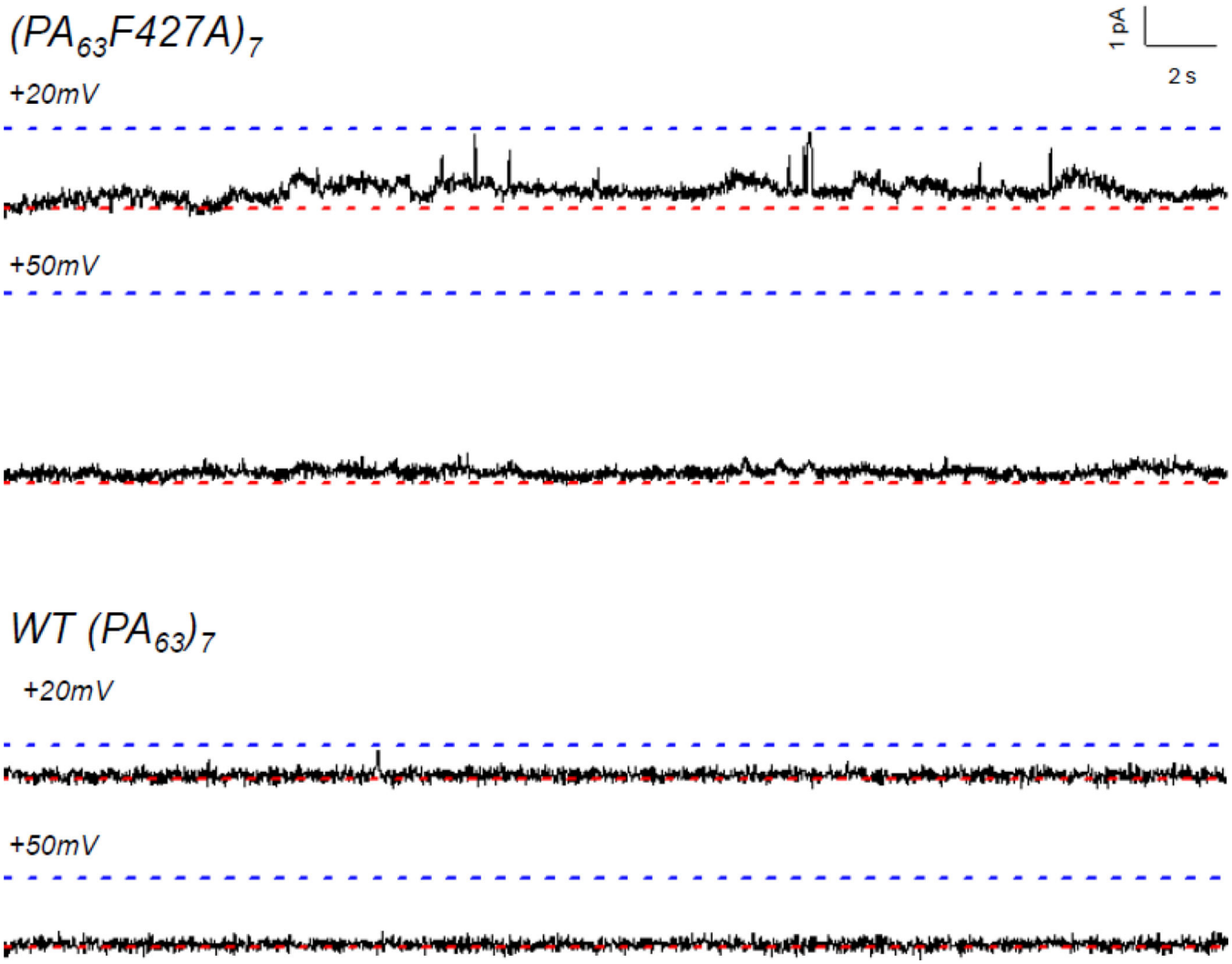

Figure 7.

Single-channel records of *cis* effect of LF_N-YFP on conductance of $(PA_{63}F427A)_7$ (top) and WT $(PA_{63})_7$ (bottom) channels at +20 mV and +50 mV. For each record, the upper dashed blue line represents the open state and the lower dashed red line represents the completely blocked (or closed) state. (The open-state conductance of the mutant channel is roughly double that of the WT channel at both +20 mV and +50 mV.) Note that the conductance of the WT $(PA_{63})_7$ channel is completely blocked by LF_N-YFP, whereas there is a small residual conductance at both +20 mV and +50 mV in the $(PA_{63}F427A)_7$ channel. Records are 35 seconds long and filtered at 15 Hz.

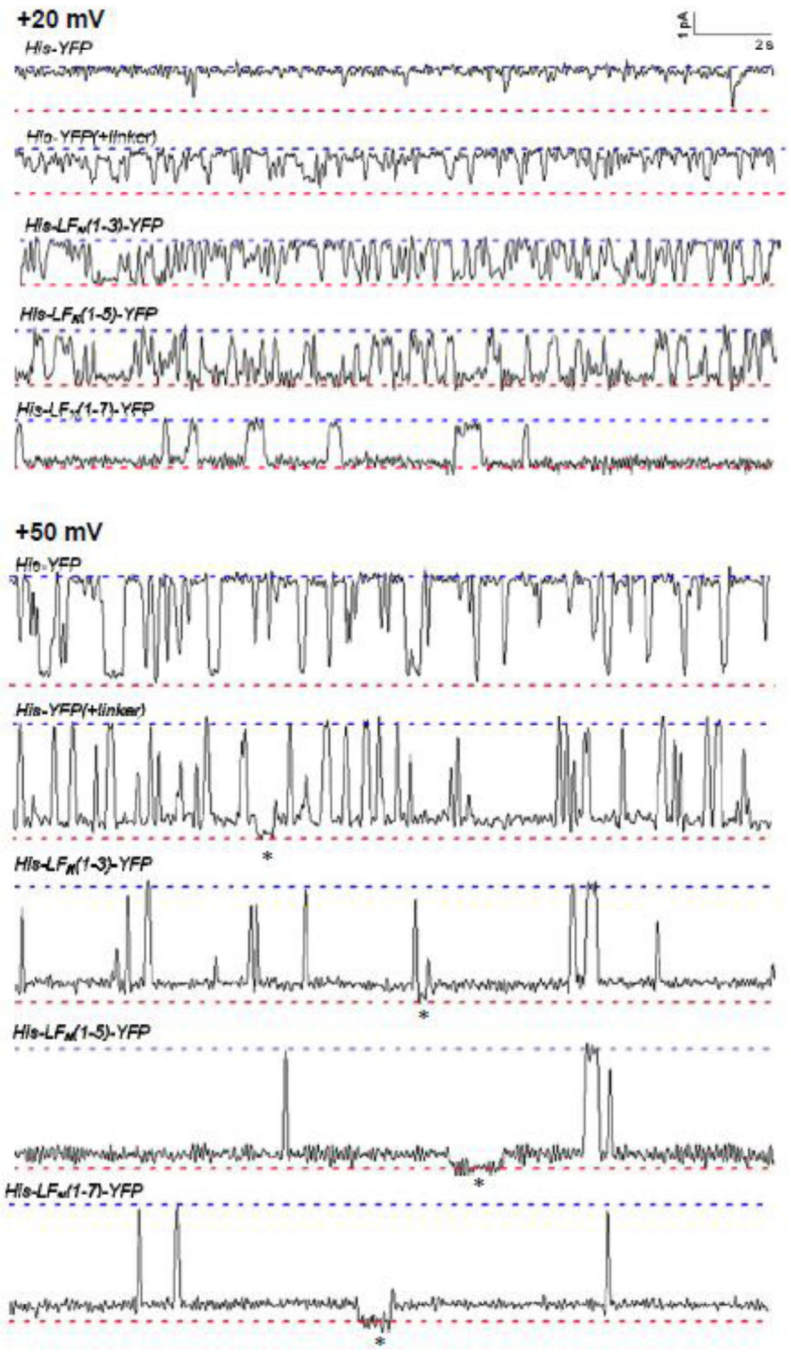

Figure 8.

Single-channel records of the *cis* effect of selected truncated His-LF_N-YFP constructs on the conductance of $(PA_{63}F427A)_7$ channels at +20 mV (*top*) and +50 mV (*bottom*). For each construct, the upper dashed blue line represents the open state and the lower dashed red line represents the completely blocked (or closed) state. Note the incomplete block at +50 mV; the asterisks indicate the brief moments where a given channel enters a completely blocked (or closed) state. Also note that the conductance fluctuations are reminiscent of those seen with tethered DNA[26]. Records are 20 seconds long and filtered at 10 Hz.

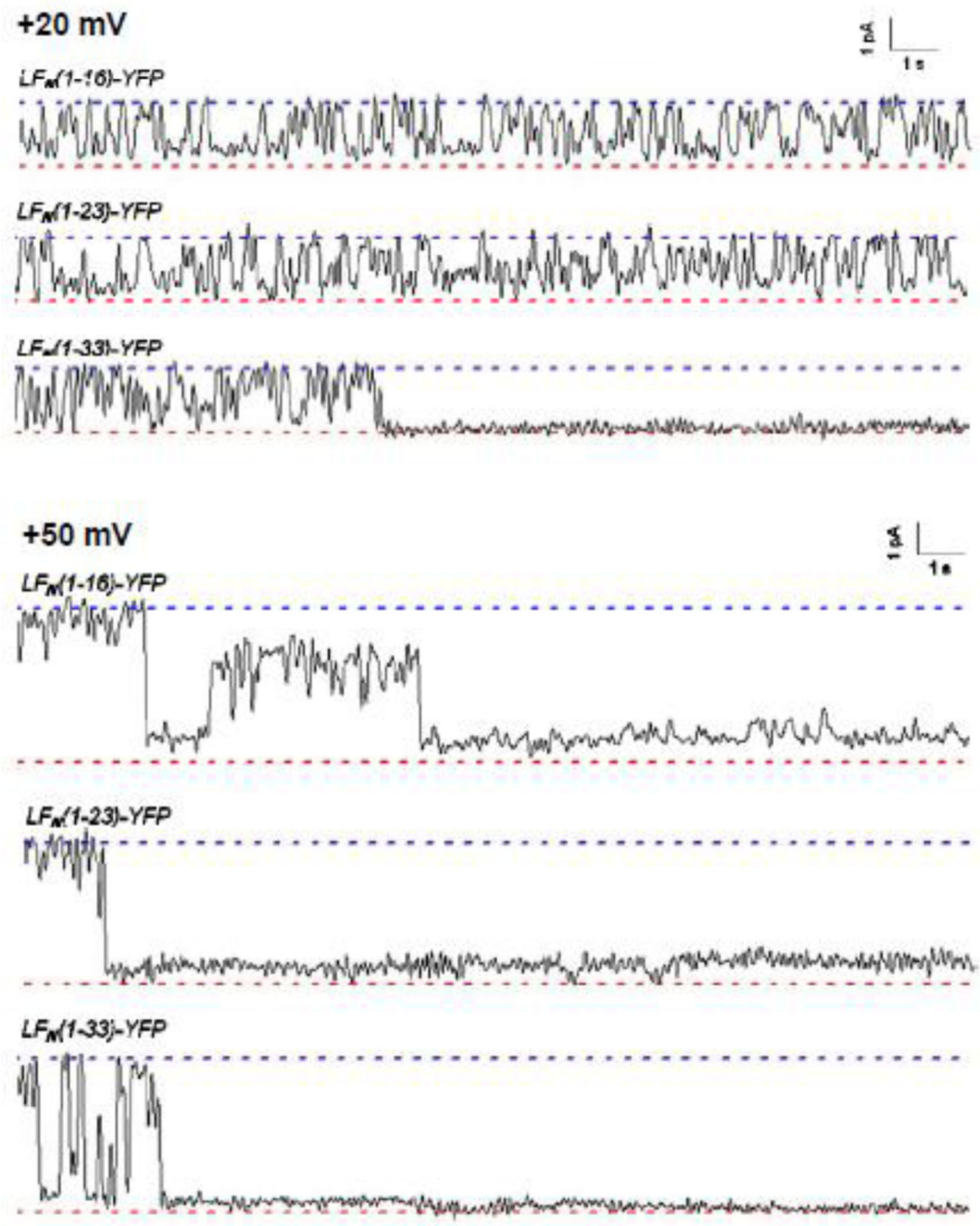

Figure 9.

Single-channel records of the *cis* effect of truncated LF_N-YFP constructs on the conductance of $(PA_{63}F427A)_7$ at +20 mV (*top*) and +50 mV (*bottom*). For each construct, the upper dashed blue line represents the open state and the lower dashed red line represents the completely blocked (or closed) state. Records are 20 seconds long and filtered at 10 Hz. In the record for LF_N(1–33)-YFP at +20 mV, there was subsequent unblocking later on.

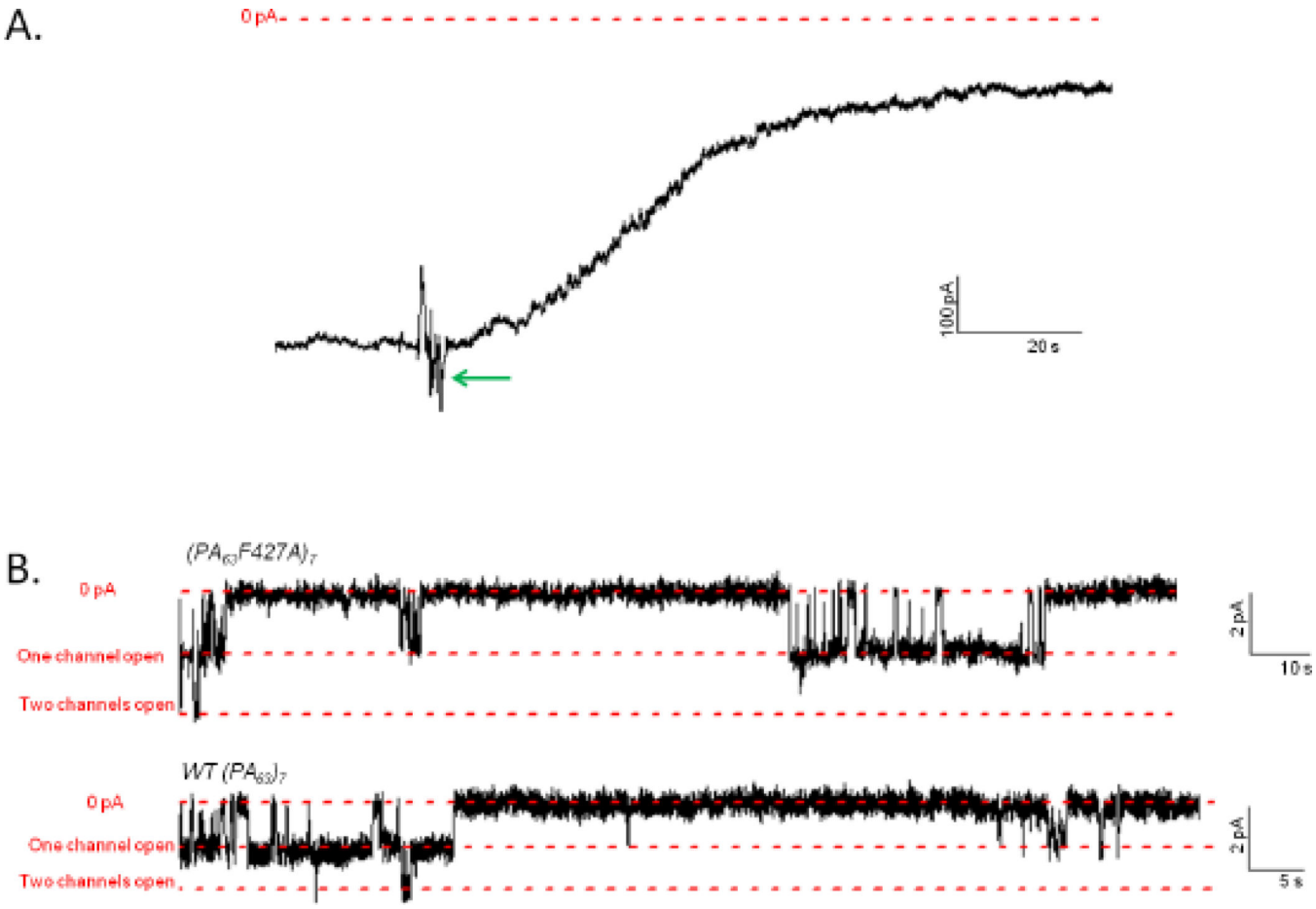

Figure 10.

A. Record of *trans* addition of 0.47 μM His-YFP to a membrane containing $(PA_{63}F427A)_7$ channels. After the current (shown as a black line) produced by $(PA_{63}F427A)_7$ channels reached a steady state at −20 mV, His-YFP was added at the green arrow (voltage held at −20 mV), reducing the current by a factor of ~6. The zero baseline of current is shown as a dashed red line. **B**. Single-channel records of the *trans* effect of His-YFP on the conductance of membranes containing two $(PA_{63}F427A)_7$ channels (*top*) and two WT $(PA_{63})_7$ channels (*bottom*) at −20 mV. Subsequent unblocking at +20 mV (not shown) confirmed that both channels were still present. The three dashed red lines in each record represent, respectively, the zero baseline of conductance, the open state conductance of one channel, and the open state conductance of two channels. Top record is 170 seconds long and bottom record is 90 seconds long; both are filtered at 10 Hz.

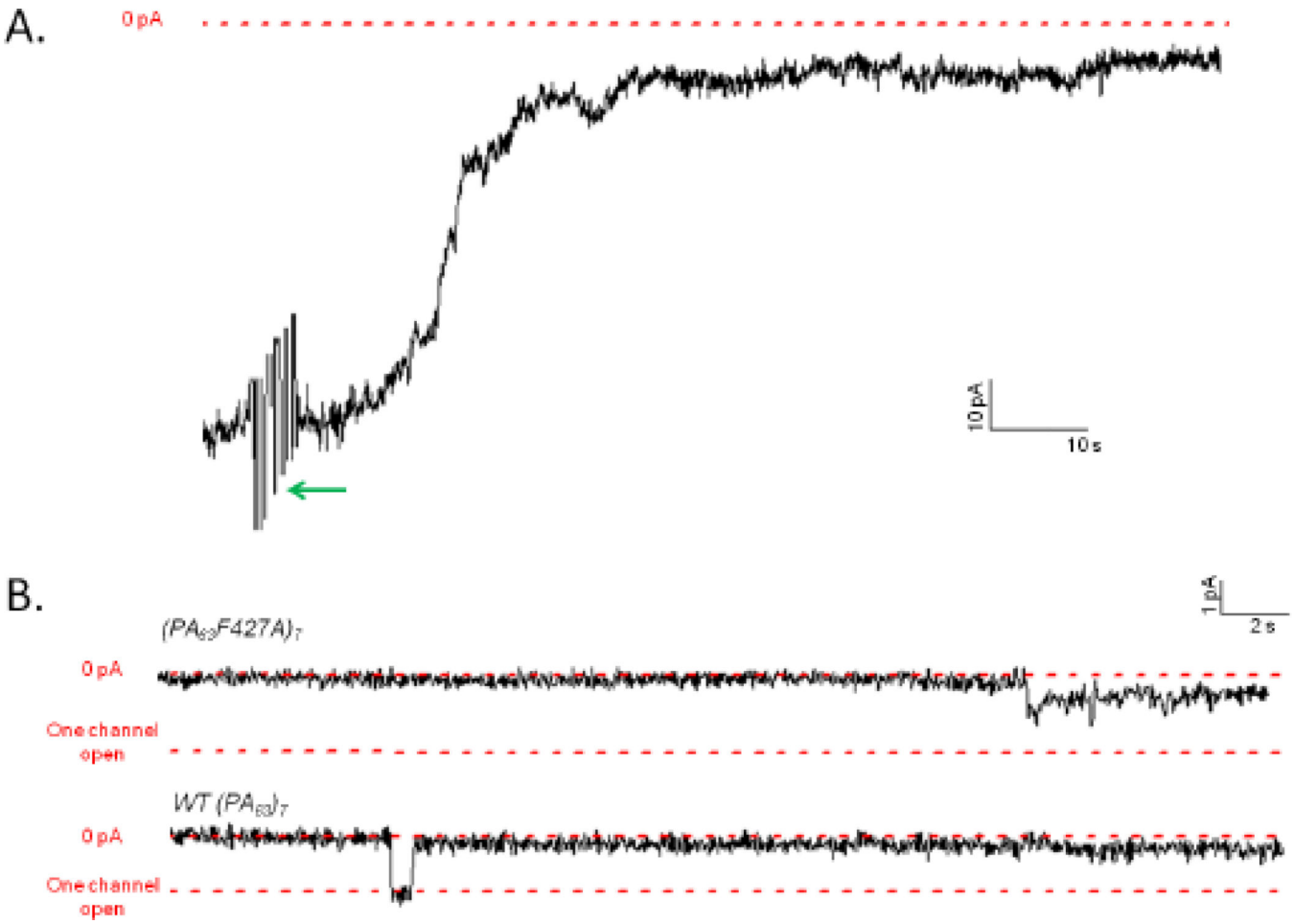

Figure 11.

A. Record of *trans* addition of 0.47 μM LF_N(1–16)-YFP to a membrane containing $(PA_{63}F427A)_7$ channels. After the current (shown as a black line) produced by $(PA_{63}F427A)_7$ channels reached a steady state at −20 mV, LF_N(1–16)-YFP was added at the green arrow (voltage held at −20 mV), reducing the current by a factor of ~11. The zero baseline of current is shown as a dashed red line. **B**. Single-channel records of the *trans* effect of LF_N(1–16)-YFP on the conductance of membranes containing one $(PA_{63}F427A)_7$ channel (*top*) and one WT $(PA_{63})_7$ channel (*bottom*) at −20 mV. Note the intermediate substates in both records. (The intermediates are smaller in the WT channel as its conductance is roughly half that of the mutant channel.) Subsequent unblocking at +20 mV (not shown) confirmed that the channel was still present. The two dashed red lines in each record represent, respectively, the zero baseline of conductance and the open state conductance of one channel. Record is 35 seconds long and filtered at 10 Hz.